

AM Bench 2025 Measurements and Challenge Problems

Modelers are invited to submit challenge problem simulation results before the deadline of 23:59 (ET) on August 29, 2025. There are no restrictions on what challenge problems are attempted. For each set of benchmarks, a downloadable .pdf file is provided that describes all the measurements and challenge problems. Tabulated results using challenge-specific templates are required for most challenges. Because some participants may not be able to share proprietary details of the modeling approaches used, we are not requiring such details. However, whenever possible we strongly encourage participants to include with their submissions a .pdf document describing the modeling approaches, physical parameters, and assumptions used for the submitted simulations.

All evaluations of submitted modeling results will be conducted by the AM Bench 2025 Organizing Committee in conjunction with the relevant AM Bench 2025 measurement teams. Award plaques will be awarded at the discretion of the Organizing Committee.

If you are interested in following or participating in any of the AM Bench 2025 challenge problems, please email us at ambench@nist.gov so we can add you to our contact list. This will allow us to inform you if any updates are made.

Please note that the challenge problems reflect only a small part of the validation measurement data provided by AM Bench for each set of benchmarks. The Measurement Description sections for each set of benchmarks describe the full range of measurements conducted.

Challenge Problems

AMB2025-08: Phase transformation sequence within single laser tracks on Fe-Cr-Ni alloys

- **Phase Transformation Sequence (CHAL-AMB2025-08-PTS):** Predict the time sequence of phases that evolve during and after solidification.
- **Phase transformation kinetics (CHAL-AMB2025-08-PTK):** Whereas the previous challenge focuses on identifying the order of phase formation, this part of the challenge requires predicting the rates and mechanisms by which these transformations occur.

1. Overview and Basic Objectives

The primary objective of AMB2025-08 is to understand the phase transformation sequence that occurs during the laser-melting-induced solidification of Fe-Cr-Ni alloys with varying Cr/Ni ratios. AM of metals inherently involves rapid heating and cooling cycles, leading to highly nonequilibrium solidification conditions. Such conditions can result in unique microstructures and phase formations that are not commonly observed in traditional manufacturing processes. The microstructural evolution in metal AM is highly sensitive to processing parameters, such as laser power, scan speed, and layer thickness, as well as the material's composition. Hence, a comprehensive understanding and the ability to accurately model phase transformations under AM's dynamic processing conditions are critical for process development and optimization.

In this Challenge, we employ state-of-the-art, synchrotron-based, high-speed X-ray diffraction measurements during single-track laser-melting experiments of Fe-Cr-Ni alloys to capture real-time data on phase evolution. The objective of this Challenge is to provide rigorously obtained, high-fidelity data to serve as the ground truth to benchmark computation models, facilitate the validation and improvement of computational models predicting phase transformations, and support the development of predictive modeling approaches for AM process optimization.

2. Material Description

We prepared ternary Fe-Ni-Cr samples for the high-speed X-ray diffraction experiments. An external vendor was sourced to produce these materials using high-purity iron (Fe), nickel (Ni), and chromium (Cr) with a nominal composition of 70 wt % Fe and Cr/Ni ratios ranging from 1.5 to 1.8, as shown in Table 1. The materials were melted using a vacuum arc melting system, ensuring complete mixing in an inert atmosphere. Each 500 g ingot underwent multiple remelting cycles to mitigate compositional gradients.

Table 1. Nominal designed composition of the ternary alloys. All values in the table are in wt %.

| Cr/Ni ratio | Fe | Cr | Ni |
|--------------|----|--------|--------|
| Cr/Ni = 1.50 | 70 | 18 | 12 |
| Cr/Ni = 1.60 | 70 | 18.462 | 11.538 |
| Cr/Ni = 1.65 | 70 | 18.679 | 11.321 |
| Cr/Ni = 1.80 | 70 | 19.286 | 10.714 |

Table 2. Bulk measured composition of the alloys. All values in the table are in wt % or ppm %.

| Cr/Ni ratio | Fe | Cr | Ni | C [ppm] | N [ppm] | O [ppm] | S [ppm] |
|--------------|---------|------|------|---------|---------|---------|---------|
| Cr/Ni = 1.50 | balance | 17.6 | 12.2 | 18 | 8.7 | 260 | < 5 |
| Cr/Ni = 1.60 | balance | 18.0 | 11.7 | 19 | 18 | 280 | 7.7 |
| Cr/Ni = 1.65 | balance | 18.2 | 11.5 | 40 | 30 | 240 | 7.9 |
| Cr/Ni = 1.80 | balance | 18.7 | 11.0 | 13 | 8.9 | 320 | 5.1 |

Table 2 shows the measured composition. For these measurements, the elements Cu, Mn, Mo, Si, Ti, V, and H were also measured but not detected. For the measurements reported in Table 2, Heavy elements (Fe, Cr, Ni, Cu, Mn, Mo, Si, Ti, V) were analyzed using Inductively Coupled Plasma Optical Emission Spectroscopy (ICP-OES). Interstitial elements (H, O, N, C, S) were measured with Instrumental Gas Analysis (IGA). All measurements were performed by EAG Laboratories¹. Detailed information about their procedures is available on their website. The measured compositions were obtained after subsequent heat treatments detailed in the following paragraph.

After melting, the ingots were homogenized at 1050 °C for 36 hours to achieve uniform composition. They were then cold-rolled to a 90 % thickness reduction to refine the grain microstructure. A subsequent

¹ Certain commercial equipment, instruments, or materials (or suppliers, or software, ...) are identified in this paper to foster understanding. Such identification does not imply recommendation or endorsement by the National Institute of Standards and Technology, nor does it imply that the materials or equipment identified are necessarily the best available for the purpose.

recrystallization anneal at 1050 °C for 5 minutes relieved internal stresses and promoted the formation of small, equiaxed grains suitable for X-ray diffraction studies.

The alloy sheets were machined into rectangular specimens measuring approximately 40 mm × 5 mm × 0.3 mm. These dimensions are optimized for the reported high-speed single-track X-ray diffraction experiments based on previous experience. Prior to testing, the specimen surfaces were polished to a near-mirror finish to facilitate reproducible laser-material interaction and X-ray measurements.

3. Experimental Setup for In Situ High-Speed X-ray Diffraction

Given the nature of the highly specialized measurements required to acquire the data for this Challenge, we will use this section to describe the experimental setup in detail so that the modelers who decide to participate in this Challenge can understand the nature of the measurements. We encourage the modelers to reach out to us should they have any questions about the experiments that are not addressed in this section.

In situ, high-speed X-ray diffraction experiments were conducted at beamline 1-ID-E of the Advanced Photon Source (APS), Argonne National Laboratory. The instrument setup is shown in Figure 1.

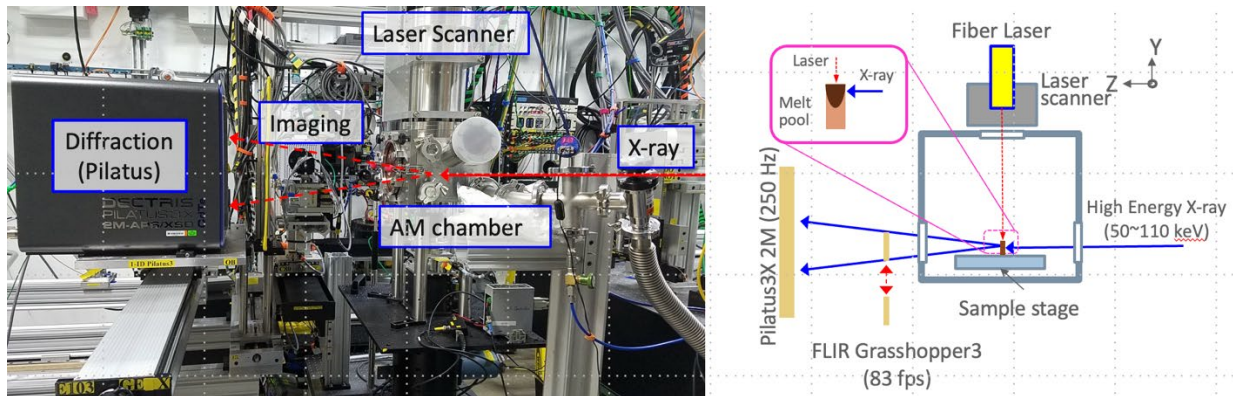


Figure 1: In situ synchrotron X-ray diffraction experiment setup. On the left is a picture of the setup inside the 1-ID-E hutch at the Advanced Photon Source. A schematic of the setup is shown on the right.

In these experiments, monochromatic X-rays, generated by an undulator source, are used to probe the internal structure of the sample during the process. The X-ray beam is first focused using a series of compound refractive lenses (CRL), which focus the X-rays to a stable focal point for high-resolution diffraction measurements so that the interaction between the X-rays and the material can be accurately measured.

The sample is positioned within a custom-designed AM chamber developed at the APS, specifically engineered to accommodate both the X-ray imaging and diffraction system as well as a high-power laser source for material processing. This rectangular stainless-steel vacuum chamber contains multiple ports that facilitate beam entry and exit, along with in situ monitoring capabilities.

For the current challenge, the relevant ports include a 3-inch port on the X-ray incident side, allowing the X-ray beam to enter the chamber, and a 6-inch port on the opposite side, enabling the diffracted X-rays to exit with minimal attenuation. To maintain environmental integrity while minimizing diffraction

interference, Kapton film was used as the window material for these ports, as it is amorphous and does not contribute to the diffraction intensity other than minimally adding to the background signal.

During the experiments, the chamber was first evacuated using a vacuum pump and then backfilled with high-purity argon. This evacuation and backfill process was repeated to ensure an inert environment for the experiment.

The chamber is equipped with a vertical stage featuring a large motion range, allowing precise positioning relative to the X-ray beam. The specimen holder consists of motorized stages providing three degrees of freedom (translation along the X, Y, and Z axes) for fine adjustments. The laser is delivered via a scanner mounted on top of the chamber, as shown in Figure 1, enabling precise beam control during material processing.

The laser used in this setup is a 520-watt ytterbium fiber laser (IPG YLR-500-AC) that operates at a wavelength of 1070.425 nm, with a full width at half maximum (FWHM) of 4.328 nm. This laser is capable of delivering energy input to the AM process at a range of laser energy settings and scan speeds, making it suitable for identifying the correct experimental conditions to investigate the melting and solidification behaviors of a range of materials. This laser beam has a Gaussian profile. The calibrated beam profile is shown in Figure 2. The calibrated laser spot size for the measurements is provided later in the Measurement Description section.

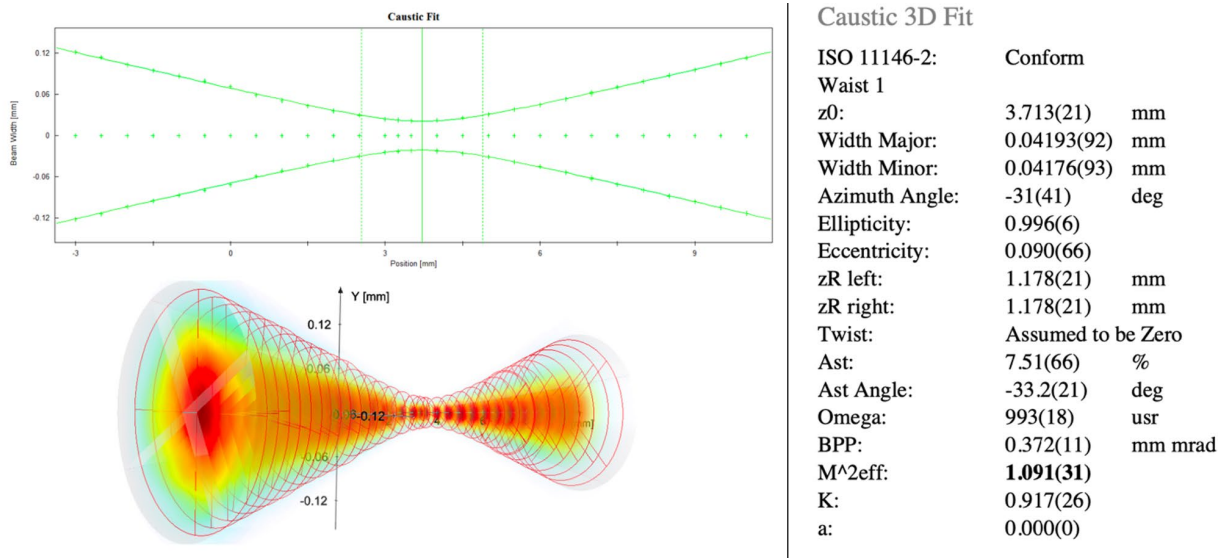


Figure 2 Laser beam profile. The measurement was done with CINOGY's focus beam profilers (FBP-2KF) by placing it at the specimen position inside the AM chamber in Figure 1.

To control the movement of the laser beam across the sample surface, a high-precision laser scanner, the ScanLab intelliSCANde® 30, is employed. This scanner utilizes a galvanometer-based system, where mirrors are rapidly adjusted to steer the laser beam with accuracy and speed. The scanning process is programmed to follow specific patterns, allowing the laser to selectively process different regions of the sample as needed. In our studies, we used the linear scan, the simplest scan strategy, to produce the high-fidelity data required for this AM Bench Challenge and to provide modelers with the best opportunity to model

the key physical phenomenon underlying this challenge, far-from-equilibrium phase transformation driven by solidification during an AM build.

For the experiments conducted in this Challenge, we used a monochromatic X-ray with an energy of 61.332 keV. The X-ray energy is calibrated using a ytterbium foil. An aluminum CRL with an aperture size of approximately 450 μm is employed to focus the X-ray beam. At the sample position, the focused X-ray beam size is 32 μm (FWHM) horizontally and 26 μm (FWHM) vertically.

An X-ray radiography imaging system is placed immediately downstream of the process chamber to capture full-field X-ray images. The full field of view of the camera is 1920 \times 1200 pixels (2.25 mm \times 1.41 mm), with a resolution of 1.172 $\mu\text{m}/\text{pixel}$ and a maximum frame rate of 82 Hz. We use this imaging system for alignment of the X-ray beam position during an experiment.

A Pilatus3 X 2M CdTe X-ray area detector is used to collect diffraction signals during the experiment. This photon-counting detector has an active area of 254 \times 289 mm² (1475 \times 1679 pixels), with a pixel size of 0.172 \times 0.172 mm². The maximum acquisition rate at full field is 250 Hz, which was used throughout the experiment.

4. Measurement Descriptions

Before collecting the diffraction data, the samples were placed inside the chamber and X-ray imaging was used to precisely position the beam, as shown in Figure 3.

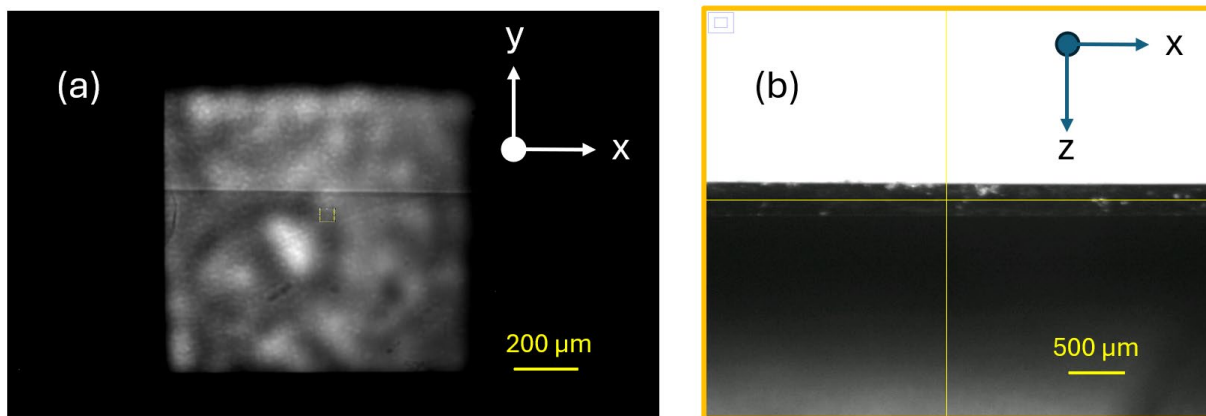


Figure 3(a): X-ray radiography image showing the location of the X-ray beam inside the sample during the experiment; (b) top-view optical imaging showing the laser alignment on the sample surface.

Figure 3(a) is an X-ray radiography image taken from the xy-plane, where the z-axis is parallel to the incident X-ray beam direction. The straight line cutting across the radiograph represents the top surface of the sample, enhanced by X-ray phase contrast. The yellow square in the middle indicates the location of the focused beam during the single-track experiment. The beam is positioned 50 μm below the top surface of the sample and remained stationary throughout the experiment.

Figure 3(b) presents a top-view of the sample before the experiment began. The sample positioning system was aligned so that the crosshair indicates the midpoint of the sample in the z-direction, while the horizontal line represents the laser scan path in the x-direction. Prior to each melting experiment, the

specimen was positioned to ensure that the laser beam center coincided with the sample midpoint. The laser path was aligned to remain centered on the sample during scanning.

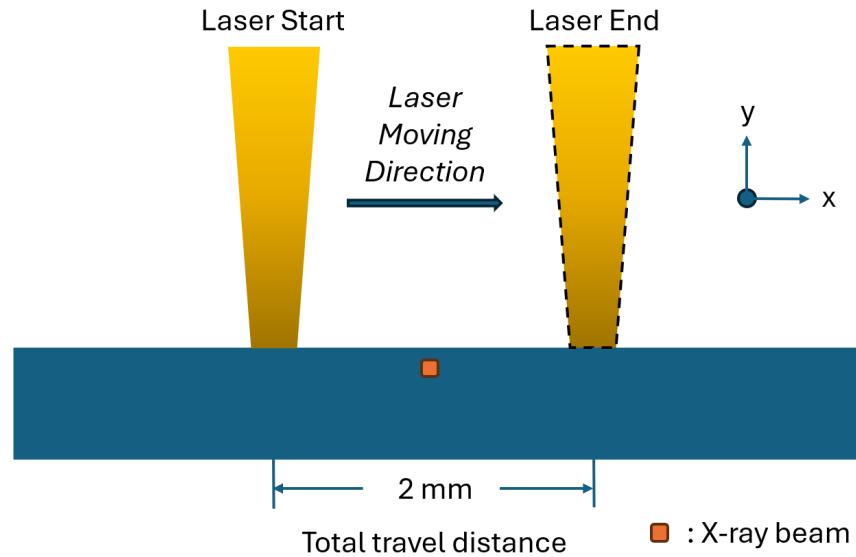


Figure 4: Schematic showing the single-track experiments for this Challenge.

Figure 4 illustrates the single-track experiment for this Challenge. Here, the laser scans linearly along on the sample at specified start and end points resulting in a total travel distance of 2 mm. The X-ray observation window was positioned at the midpoint of this path, i.e., at the 1 mm mark, and at a depth of 50 μm .

As the laser moves across the specimen, the material within the diffracted region rapidly melts and then resolidifies due to the motion of the melt pool (not shown in this figure), causing changes in the diffraction pattern. Experiments were conducted at two laser scan speeds (0.01 m/s and 0.1 m/s) for all four materials in order to affect an order of magnitude difference in solidification conditions. Diffraction patterns are collected via transmission during the entirety of the laser scanning process.

The diffraction patterns reveal the phase transformation sequence from the liquid melt pool to room temperature. For each experiment included in this Challenge, we captured 1,000 frames of diffraction patterns at 250 Hz to ensure the complete transformation sequence was recorded. For each frame, the exposure time of the detector was 0.02 s, striking a balance between the signal-to-noise and resolution of the transformation kinetics.

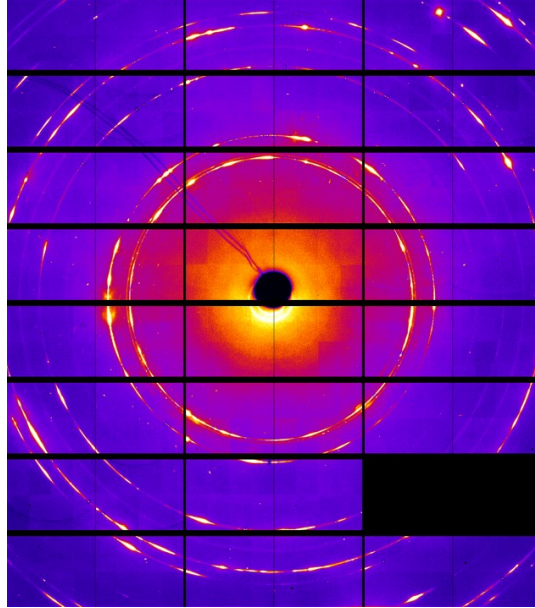


Figure 5: An example of the HEXRD pattern of the test materials used in this Challenge.

Figure 5 shows the diffraction pattern acquired before a single-track experiment. The detector consists of 24 individual detecting modules, with one module non-functional and gaps between neighboring modules. During the data reduction and analysis process, we applied masks to ensure that the missing module and gaps did not affect the results. All results used to benchmark this Challenge originate from time-resolved diffraction patterns like the one shown in Figure 5. The diffraction data were calibrated using the NIST standard reference material SRM 674b (CeO₂).

Table 3: Measurement parameters of the high-speed diffraction experiments for this Challenge.

| Material | Thickness (mm) | Laser Power (W) | Laser Scan Velocity (m/s) | Laser Spot Size (μm) |
|--------------|----------------|-----------------|---------------------------|----------------------|
| Cr/Ni = 1.50 | 0.30 ± 0.04 | 65 | 0.01 | 108 |
| Cr/Ni = 1.50 | 0.30 ± 0.04 | 135 | 0.1 | 108 |
| Cr/Ni = 1.60 | 0.40 ± 0.01 | 65 | 0.01 | 108 |
| Cr/Ni = 1.60 | 0.40 ± 0.01 | 140 | 0.1 | 108 |
| Cr/Ni = 1.65 | 0.29 ± 0.03 | 70 | 0.01 | 108 |
| Cr/Ni = 1.65 | 0.29 ± 0.03 | 135 | 0.1 | 108 |
| Cr/Ni = 1.80 | 0.30 ± 0.03 | 85 | 0.01 | 108 |
| Cr/Ni = 1.80 | 0.30 ± 0.03 | 180 | 0.1 | 108 |

Table 3 shows the laser parameters for the benchmark measurements. Here, we fine-tuned the laser power to ensure that the material inside the observation is fully melted and the complete phase transformation sequence was captured.

We also performed phase fraction analysis on the materials prior to the high-speed diffraction experiments using a 500 μm × 500 μm X-ray beam. An example diffraction pattern is shown in Figure 5. These materials are predominantly austenitic, with the austenite fraction exceeding 95 % by volume based on diffraction

data from the bulk specimen. The lattice parameters of the austenite in these samples are reported in Table 4.

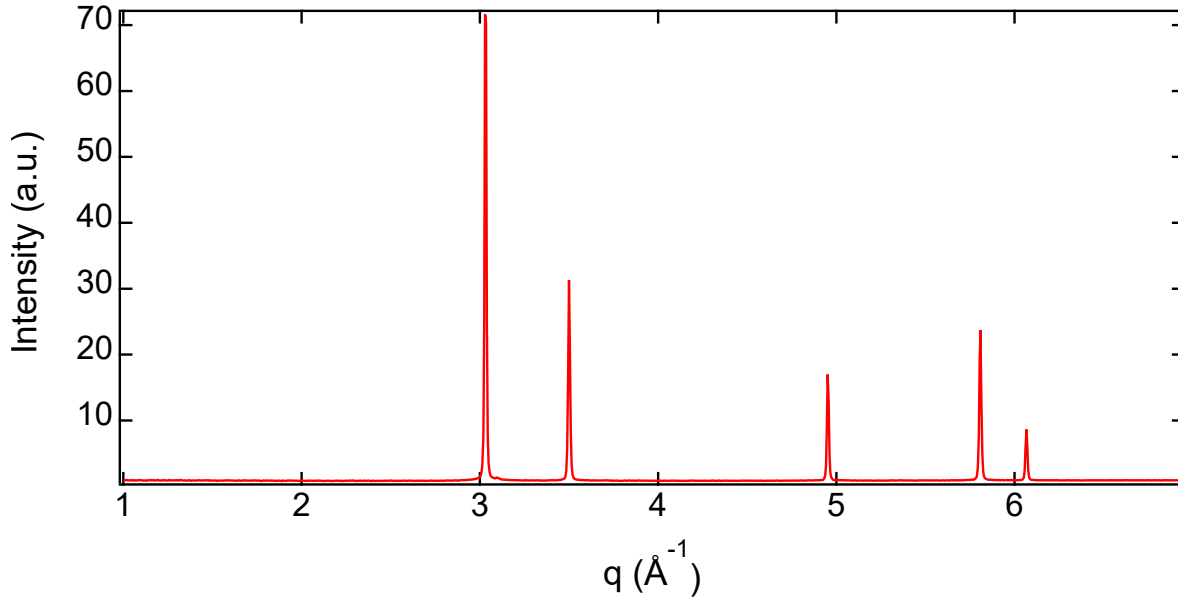


Figure 6: An example of the 1D diffraction pattern of the materials studied in the Challenge. In this material ($Cr/Ni = 1.65$), the diffraction pattern is primarily austenitic.

Table 4: Lattice parameters for the starting materials.

| Material | FCC lattice parameter (Å) |
|--------------|---------------------------|
| Cr/Ni = 1.50 | 3.5848 ± 0.0005 |
| Cr/Ni = 1.60 | 3.5846 ± 0.0004 |
| Cr/Ni = 1.65 | 3.5855 ± 0.0003 |
| Cr/Ni = 1.80 | 3.5852 ± 0.0005 |

4. Benchmark Challenge Problems

4.1 Phase Transformation Sequence (CHAL-AMB2025-08-PTS)

For this challenge, the modelers are expected to predict the phase transformation sequence from the molten state of the material during the solidification process. Specifically, they should determine which phases appear first, what subsequent phases emerge, and whether any phases undergo further transformation. The focus is on identifying the order of phase formation rather than the kinetics of transformation.

Key expectations include:

- Predicting the first solid phase to form upon solidification.
- Identifying whether intermediate metastable phases appear before reaching a stable phase.
- Determining the final equilibrium phase at room temperature.

- Assessing whether any phases persist, disappear, or transform into new phases as cooling progresses.

This analysis will help establish the fundamental phase evolution pathway from liquidus to room temperature (20 °C) without requiring an explicit time-dependent description of transformation kinetics, which is addressed in the next part of the challenge.

4.2 Phase transformation kinetics (CHAL-AMB2025-08-PTK)

For this challenge, the modelers are expected to predict how the identified phases evolve as a function of time during and after solidification. Unlike the previous phase transformation sequence task, which focuses on identifying the order of phase formation, this part of the challenge requires predicting the rates and mechanisms by which these transformations occur.

Key expectations include:

- Time-resolved tracking of phase evolution, from the initial solidification stage to the final room temperature structure.
- Predicting phase fractions as a function of time, capturing the rate at which each phase forms, grows, or disappears.
- Modeling solid-state phase transformations, including any diffusion-controlled transformations or other non-equilibrium transformations.
- Evaluating the influence of cooling rate and processing parameters (e.g., laser power, scan speed) on transformation kinetics.

A successful model in this category should not only capture the final phase composition but also accurately describe how the transformation progresses over time, providing insight into the dynamic nature of phase changes in additive manufacturing conditions.

4.3 Submission templates and assessment metrics

A submission template, “Challenge -08 Submission Template,” is provided [here](#). Metrics for evaluating the submissions are still being evaluated and this part of the description document will be updated shortly.

5. Relevant References

- (1) Babu, S.; Elmer, J.; Vitek, J.; David, S. Time-resolved X-ray diffraction investigation of primary weld solidification in Fe-C-Al-Mn steel welds. *Acta Materialia* **2002**, *50* (19), 4763-4781.
- (2) Yonemura, M.; Osuki, T.; Terasaki, H.; Komizo, Y.; Sato, M.; Kitano, A. In-situ observation for weld solidification in stainless steels using time-resolved X-ray diffraction. *Materials Transactions* **2006**, *47* (2), 310-316.
- (3) Parab, N. D.; Zhao, C.; Cunningham, R.; Escano, L. I.; Fezzaa, K.; Everhart, W.; Rollett, A. D.; Chen, L.; Sun, T. Ultrafast X-ray imaging of laser–metal additive manufacturing processes. *Synchrotron Radiation* **2018**, *25* (5), 1467-1477.
- (4) Guo, Q.; Qu, M.; Chuang, C. A.; Xiong, L.; Nabaa, A.; Young, Z. A.; Ren, Y.; Kenesei, P.; Zhang, F.; Chen, L. Phase transformation dynamics guided alloy development for additive manufacturing. *Additive Manufacturing* **2022**, *59*, 103068.

- (5) König, H.-H.; Pettersson, N. H.; Durga, A.; Van Petegem, S.; Grolimund, D.; Chuang, A. C.; Guo, Q.; Chen, L.; Oikonomou, C.; Zhang, F. Solidification modes during additive manufacturing of steel revealed by high-speed X-ray diffraction. *Acta Materialia* **2023**, *246*, 118713.
- (6) Wang, L.; Guo, Q.; Chen, L.; Yan, W. In-situ experimental and high-fidelity modeling tools to advance understanding of metal additive manufacturing. *International Journal of Machine Tools and Manufacture* **2023**, *193*, 104077.
- (7) Elmer, J.; Wong, J.; Ressler, T.; In-situ observations of phase transformations during solidification and cooling of austenitic stainless steel welds using time-resolved x-ray diffraction. *Scripta Materiala* **2000**, *751*.